On simulation of local fluxes in molecular junctions

Gabriel Cabra,[1] Anders Jensen,[2] and Michael Galperin[1,*]

[1]*Department of Chemistry & Biochemistry,*
University of California San Diego, La Jolla, CA 92093, USA

[2]*Department of Chemistry, University of Copenhagen, 1165 København, Denmark*

Abstract

We present a pedagogical review of current density simulation in molecular junction models indicating its advantages and deficiencies in analysis of local junction transport characteristics. In particular, we argue that current density is a universal tool which provides more information than traditionally simulated bond currents, especially when discussing inelastic processes. However, current density simulations are sensitive to choice of basis and electronic structure method. We note that discussing local current conservation in junctions one has to account for source term caused by open character of the system and intra-molecular interactions. Our considerations are illustrated with numerical simulations of a benzenedithiol molecular junction.

* migalperin@ucsd.edu

I. INTRODUCTION

Since its theoretical prediction [1] molecular electronics witnessed fast progress in experimental techniques. In the last decade number of ways to characterize response of open single molecule junctions and accuracy of measurements increased dramatically. Experimental techniques available today allow to measure elastic and inelastic currents, noise, optoelectronic, thermo-electric, and magneto-electric responses in junctions. Majority of these measurements characterize response of a junction as a whole. Recently, local junction characteristics either by local probe measurement or via assigning local characteristics to particular degrees of freedom (e.g., vibrationally resolved effective temperature) started to attract attention [2–9]. Visualization at molecular scale is another window into local junction properties [10–12].

Theoretical characterization of local junction properties has its own history, and many studies of local molecular properties were instrumental in understanding overall molecular response. In particular, significant number of studies utilized bond currents as a tool illustrating effects of quantum coherence in molecules [13–19]. Bond currents, although helpful, suffer from two significant shortcomings. First, exact formulation of bond currents is possible in non-interacting systems only: any interaction mixes different bond contributions, only approximate treatment is possible in this case [16, 18]. Second, bond currents are good indicators of charge (and, possibly, also energy) flow only when the flow is dominated by through-bonds paths.

A more general description utilizes local currents (current density). Only few works studied local currents in molecular junctions [20, 21]. Preference of bond currents is due to direct connection of the latter to current divergency and hence to electron kinetic energy operator; the latter explicitly enters Green function equation-of-motion, which makes bond current evaluation an easy task. Here we present a pedagogical review of simulation of local currents in molecular junctions, and discuss advantages and shortcomings of the concept. We also indicate misconceptions about current density simulations in junctions.

Structure of the paper is the following. In Section II we introduce a model of molecular junction and give brief introduction to simulation of local currents. Numerical results and discussion are presented in Section III. Section IV summarizes our findings and outlines goals for future research.

II. MODEL AND METHOD

First, we introduce a model of molecular junction and give a short review of standard non-equilibrium Green function (NEGF) method. After that, we discuss definition of local current, its expression in terms of NEGF, and local current conservation conditions.

A. Molecular junction model

We consider junction consisting of a molecule M attached to two contacts L and R (see Fig. 1). All interactions are assumed to be confined to molecular part; contacts are reservoirs

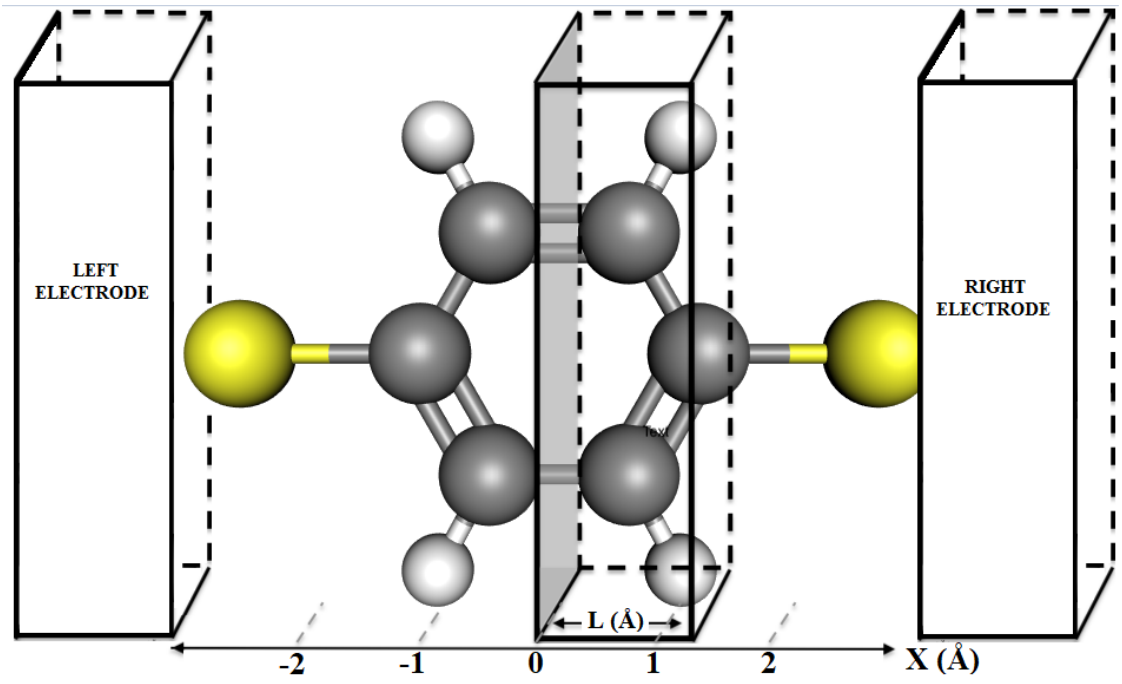

FIG. 1. Sketch of molecular junction.

of free charge carriers each at its own equilibrium. Hamiltonian of the junction is

$$\hat{H} = \hat{H}_M + \sum_{K=L,R} \left(\hat{H}_K + \hat{V}_{KM}\right) \tag{1}$$

$$\hat{H}_M = \hat{H}_M^{(0)} + \hat{H}_M^{(1)} \tag{2}$$

$$\hat{H}_K = \sum_{k\in K} \varepsilon_k \hat{c}_k^\dagger \hat{c}_k \tag{3}$$

$$\hat{V}_{KM} = \sum_{k\in K} \sum_{m\in M} \left(V_{km} \hat{c}_k^\dagger \hat{d}_m + H.c.\right) \tag{4}$$

Here $\hat{H}_M$ and $\hat{H}_K$ $(K = L, R)$ are the molecular and contacts Hamiltonians, and $\hat{V}_{MK}$ is coupling between parts of the system. $\hat{H}_M^{(0)}$ is non-interacting part of the molecular Hamiltonian and $\hat{H}_M^{(1)}$ contains all the intra-molecular interactions. $\hat{d}_m^\dagger$ $(\hat{d}_m)$ and $\hat{c}_k^\dagger$ $(\hat{c}_k)$ create (annihilate) electron in orbital m of the molecule and state k of contacts, respectively. The Hamiltonian, written in second quantization, utilizes single-electron basis $\phi_m(\vec{r})$; in quantum chemistry simulations the basis is usually chosen as atomic or molecular orbitals, or maximally localized Wannier functions. For simplicity, below we assume orthonormal basis.

Within the NEGF main object of interest is single-particle Green function defined on the Keldysh contour as (here and below $e = \hbar = m = 1$)

$$G_{m_1 m_2}(\tau_1, \tau_2) = -i\left\langle T_c\, \hat{d}_{m_1}(\tau_1)\, \hat{d}_{m_2}^\dagger(\tau_2)\right\rangle \tag{5}$$

Here T_c is the contour ordering operator and $\tau_{1,2}$ are contour variables. As usual, $G_{m_1 m_2}(\tau_1, \tau_2)$ is obtained by solving the Dyson equation

$$\left(i\partial_{\tau_1} \mathbf{I} - \mathbf{H}_M^{(0)}\right) \mathbf{G}(\tau_1, \tau_2) = \delta(\tau_1, \tau_2)\, \mathbf{I} + \int_c d\tau_3\, \Sigma(\tau_1, \tau_3)\, \mathbf{G}(\tau_3, \tau_2) \tag{6}$$

where $\mathbf{H}_M^{(0)}$, $\mathbf{G}$, and Σ are matrices in molecular subspace and $\mathbf{I}$ is unit matrix. Self-energy Σ accounts for interactions ($\mathbf{H}_M^{(1)}$ term in the Hamiltonian) and boundary conditions induced by the contacts ($\hat{H}_K$ and $\hat{V}_{MK}$ terms in the Hamiltonian)

$$\Sigma(\tau_1, \tau_2) = \Sigma^{int}(\tau_1, \tau_2) + \sum_{K=L,R} \Sigma^K(\tau_1, \tau_2) \tag{7}$$

While form of Σ^{int} depends on the nature of interactions and level of theory, explicit form for the contacts self-energies is known (see Appendix A for details).

B. Local current

For discussion below we need Green function representation in both orbital, $\{m\}$, and real space, $\{\vec{r}\}$, basis. Transition between the two is

$$G(\vec{r}_1,\tau_1;\vec{r}_2,\tau_2) = \sum_{m_1,m_2} \phi_{m_1}(\vec{r}_1)\, G_{m_1m_2}(\tau_1,\tau_2)\, \phi^*_{m_2}(\vec{r}_2) \tag{8}$$

$$G_{m_1m_2}(\tau_1,\tau_2) = \int d\vec{r}_1 \int d\vec{r}_2\, \phi^*_{m_1}(\vec{r}_1)\, G(\vec{r}_1,\tau_1;\vec{r}_2,\tau_2)\, \phi_{m_2}(\vec{r}_2) \tag{9}$$

Transferring in (6) to real space basis, taking lesser projection of the expression, and subtracting corresponding right side Dyson equation leads to the continuity equation (see Appendix B for derivation)

$$\frac{d\rho(\vec{r},t)}{dt} + \vec{\nabla}\,\vec{j}(\vec{r},t) = P(\vec{r},t) \tag{10}$$

where

$$\rho(\vec{r},t) = -i\, G^<(\vec{r},t;\vec{r},t) \tag{11}$$

$$\vec{j}(\vec{r},t) = -\frac{1}{2}\Big[\big(\vec{\nabla}_{r_1} - \vec{\nabla}_{r_2}\big) G^<(\vec{r}_1,t;\vec{r}_2,t)\Big]_{\vec{r}_1=\vec{r}_2\equiv\vec{r}} \tag{12}$$

$$P(\vec{r},t) = 2\,\mathrm{Re}\int d\vec{r}_1 \int dt_1 \Big(G^<(\vec{r},t;\vec{r}_1,t_1)\,\Sigma^a(\vec{r}_1,t_1;\vec{r},t) + G^r(\vec{r},t;\vec{r}_1,t_1)\,\Sigma^<(\vec{r}_1,t_1;\vec{r},t)\Big) \tag{13}$$

are respectively electron density, local current, and source term. Here r, $<$, and a superscripts indicate retarded, lesser, and advanced projections. Note that using electronic structure DFT simulations in prediction of local currents should be done with caution, because DFT does not provide energy resolution for self-energy due to interactions (as a result, its lesser projection is zero). This in turn affects all transport characteristics in (11)-(13) via lesser projections of Green function and self-energy, and may lead to qualitative failures even in prediction of total fluxes [22, 23] (total fluxes being integrated quantities are much less sensitive to details of simulations than current density). Note also that continuity equation (10) fixes only divergence of local current, i.e. its curl is arbitrary. This leads to question about uniqueness of definition (12). This question was discussed in the literature [24], where arguments in favor of uniqueness of definition (12) were given.

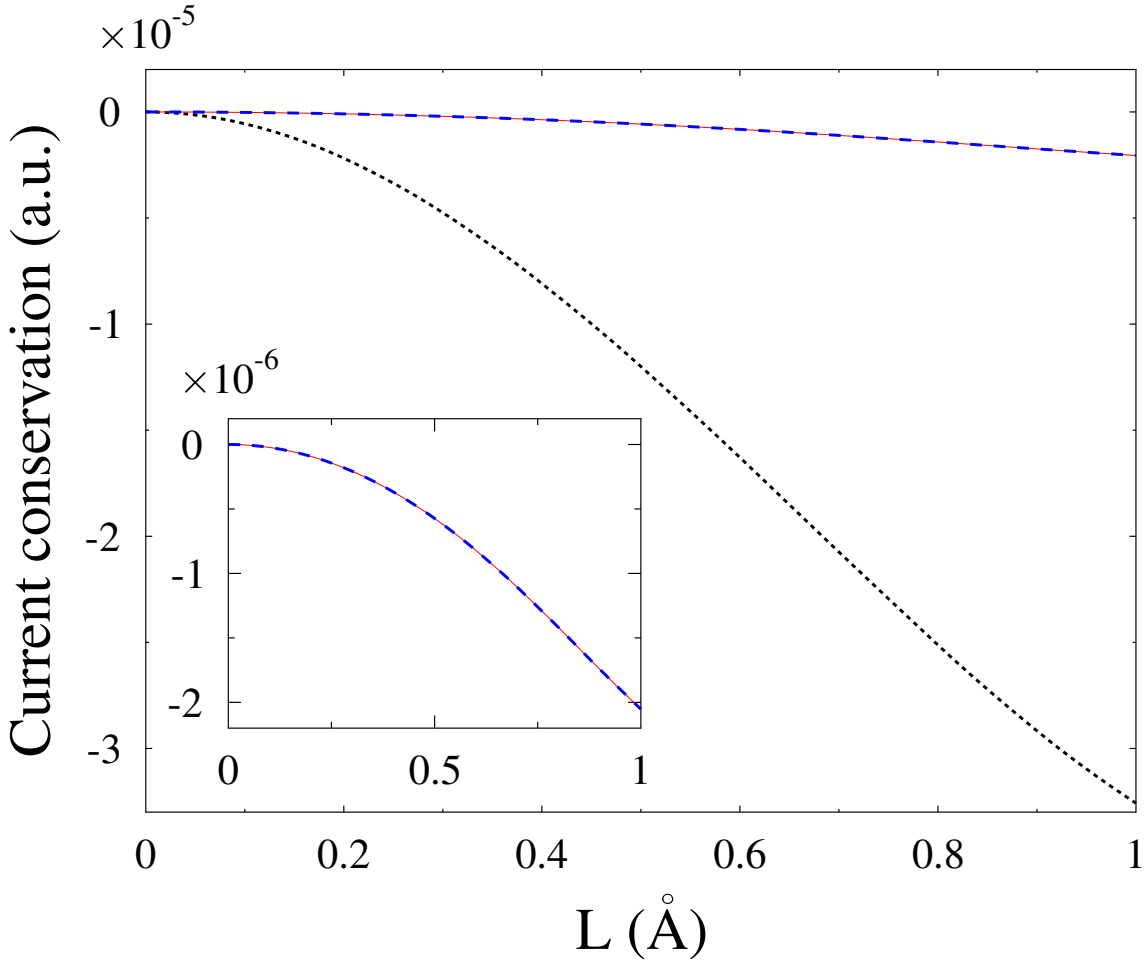

FIG. 2. Local current conservation in molecular junction of Fig. 1. Shown are integrated current flux through the surface of the slab, left side of Eq. (14), calculated in real space (Eq. (12) - integration over surface; thin dotted line, black) and orbital (Eq. (16) - integration over volume; thick dashed line, blue) basis, and integrated source term (right side of Eq. (14) represented in orbital basis; solid line, red) vs. width of the slab. Inset shows orbital basis results in higher resolution.

At steady state, junction characteristics (11)-(13) do not depend on time, so that integrating both sides of continuity equation (10) over a slab along the junction transport direction (see Fig. 1) and applying the Ostrogradsky-Gauss theorem leads to current conservation in the form

$$\oint_S d\vec{S}\,\vec{j}(\vec{r}) = \int_V d\vec{r}\,P(\vec{r}) \tag{14}$$

Here V is volume of integration and S is its surface, left side is total current balance (dif-

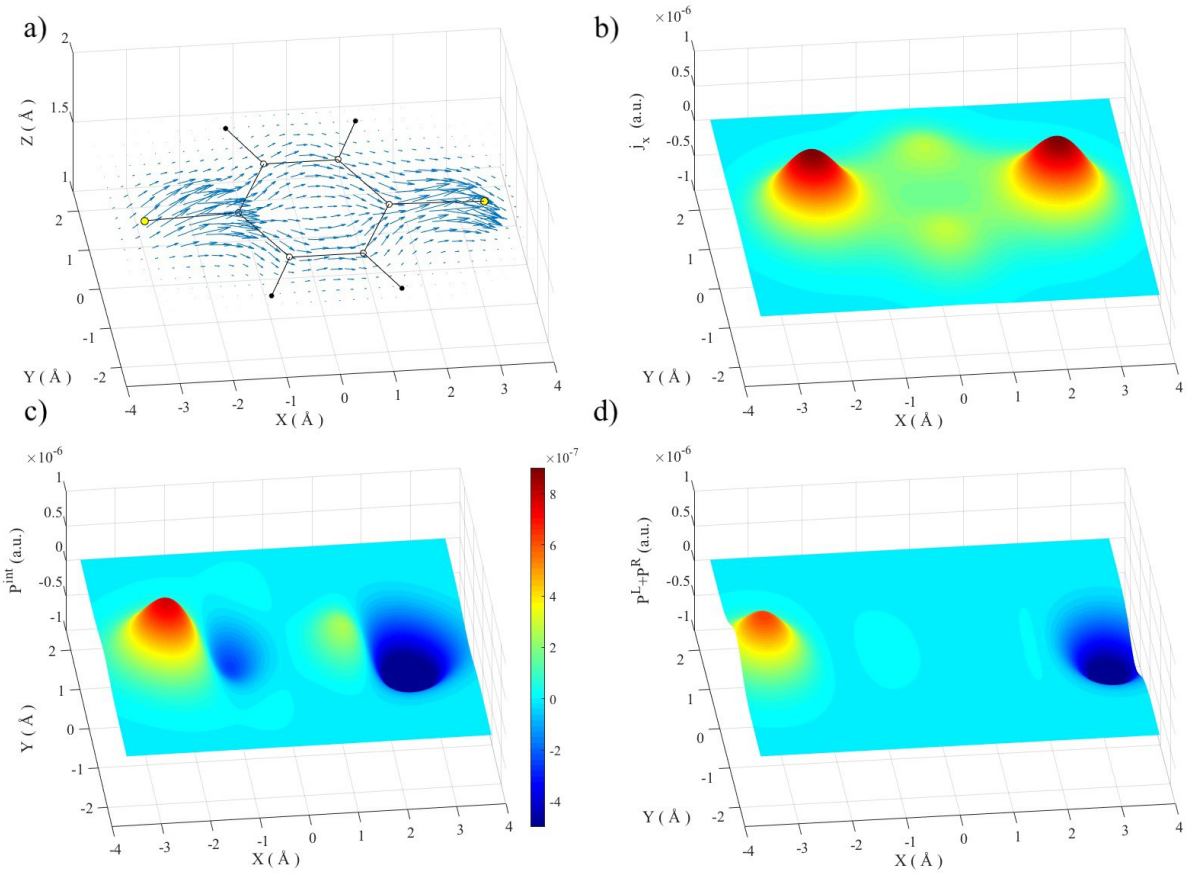

FIG. 3. Local transport characteristics of para-benzenedithiol (PBDT) molecular junction (sketched in Fig. 1) at $z = 1.5$ Å above molecular plane. Shown are (a) local current vector field (molecular structure is added as a guide to the eye); (b) map of flux along the junction (j_x) vs. position in xy plane; and maps of source terms due to electron-electron interaction (c) and contacts (d) vs. position in the xy plane.

ference between currents through right and left surfaces of the slab) while right side yields electron density production in the slab. That is, local currents within the junction are not conserved because of electron density production induced by the source term (13). It is easy to show, that extending integration in (14) to all the space results in is the usual form of current conservation $I_L - I_R = 0$, because integral over all the space of the source term is identically zero. Note however that question of current conservation due to contacts to some extent depends on representation: taking parts of contacts into account explicitly (i.e. establishing partition between system and bath farther form the molecule) will decrease effect of corresponding self-energy in the molecular subspace. The issue was discussed in Ref. [25].

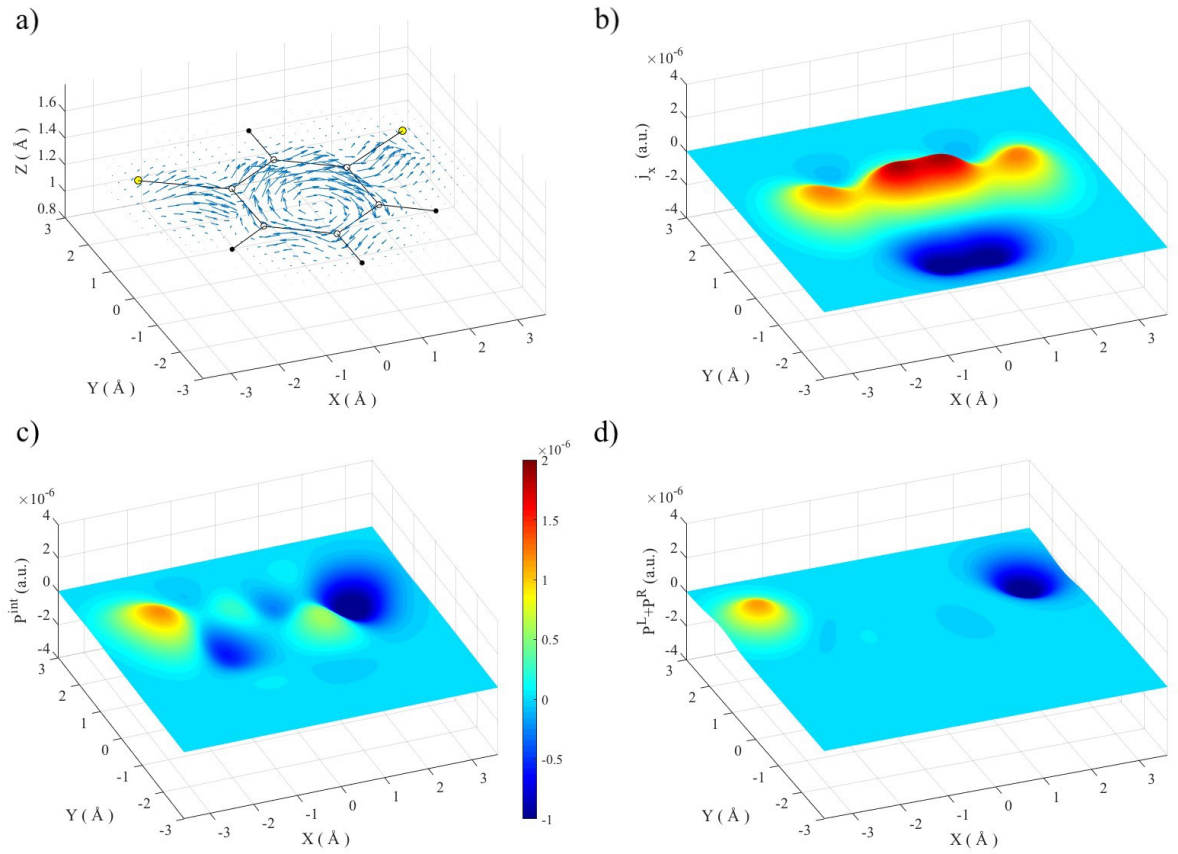

FIG. 4. Local transport characteristics of meta-benzenedithiol (MBDT) molecular junction at $z = 1.32$ Å above molecular plane. Shown are (a) local current vector field (molecular structure is added as a guide to the eye); (b) map of flux along the junction (j_x) vs. position in xy plane; and maps of source terms due to electron-electron interaction (c) and contacts (d) vs. position in the xy plane.

We note that idea of imposing local current conservation (as was suggested, e.g., in Refs. [26, 27]) is questionable. Indeed, one faces a problem of representing right side of Eq. (14) as divergence of a local flux. Because there is no strict way to define vector (local current) from scalar (source term), one has to rely on arbitrary approximations. In particular, Refs. [26, 27] assume local current being proportional to electric field which in turn is related to the source term via the Gauss law. This assumption of constant proportionality coefficient between current and field is problematic taking into account anisotropic molecular structure. Note possibility of curl in electron flux (and hence effective magnetic field) solely due to molecular anisotropy was discussed in the literature [21, 28, 29].

Besides legitimate physical reason (14) for non-conserving character of local currents, there are technical problems related to basis choice. In particular, form the two basis requirements, orthonormality $\int d\vec{r}\,\phi^*_{m_1}(\vec{r})\,\phi_{m_2}(\vec{r}) = \delta_{m_1,m_2}$ and completeness $\sum_m \phi_m(\vec{r}_1)\,\phi^*_m(\vec{r}_2) = \delta\big(\vec{r}_1 - \vec{r}_2\big)$, only the first one is satisfied in usual basis choices of quantum chemistry. As a result, transformation from orbital to real space basis, Eq. (8), does not hold. Thus, divergence of local current in real space (this expression leads to definition (12))

$$\vec{\nabla}\,\vec{j}_r(\vec{r},t) = \big[\big(H^{(0)}_M(\vec{r}_1) - H^{(0)}_M(\vec{r}_2)\big)G^<(\vec{r}_1,t;\vec{r}_2,t)\big]_{\vec{r}_1=\vec{r}_2\equiv\vec{r}}, \tag{15}$$

differs from the divergence expressed in orbital basis

$$\vec{\nabla}\,\vec{j}_{orb}(\vec{r},t) = \sum_{m_1,m_2} \phi_{m_1}(\vec{r})\big[\mathbf{H}^{(0)}_M;\mathbf{G}^<(t,t)\big]_{m_1m_2}\phi^*_{m_2}(\vec{r}) \tag{16}$$

Because source term is usually calculated from orbital representation of the Dyson equation, expression (14) will be violated simply due to incompleteness of the orbital basis. Note that convergence of the basis to completeness was discussed in Refs. [25, 30, 31].

III. RESULTS AND DISCUSSION

We now illustrate advantages and deficiencies of local current simulations in molecular junctions. Electronic structure calculations were performed using Gaussian [32] with electron-electron interaction simulated at the Hartree-Fock level of theory utilizing STO-3g basis. Retarded (equal to advanced) is the only non-zero projection of the corresponding self-energy $\Sigma^{int\,HF}(\tau_1,\tau_2)$. The projection was calculated as difference between Fock matrix and part of the Hamiltonian representing electronic kinetic energy plus its potential in nuclear frame. Fermi energy E_F was chosen 1 eV above HOMO, and bias V_{sd} was applied symmetrically: $\mu_{L,R} = E_F \pm |e|\,V_{sd}$. Unless stated otherwise, simulations were performed for $V_{sd} = 3$ V. For simplicity, contacts were represented as continuum coupled to sulphur atoms and treated within the wide band approximation. Escape rate for each orbital of sulphur atoms was taken to be the same: $\Gamma^K = 0.1$ eV ($K = L, R$). We note that our results are for illustration purposes only; first principles analysis should employ better basis and include *ab initio* simulations of self-energies due to coupling to contacts.

Figure 2 illustrates conservation of local current, Eq. (14), vs. width L of a slab (see Fig. 1). As expected, with the slab approaching area of contacts (area where source term is

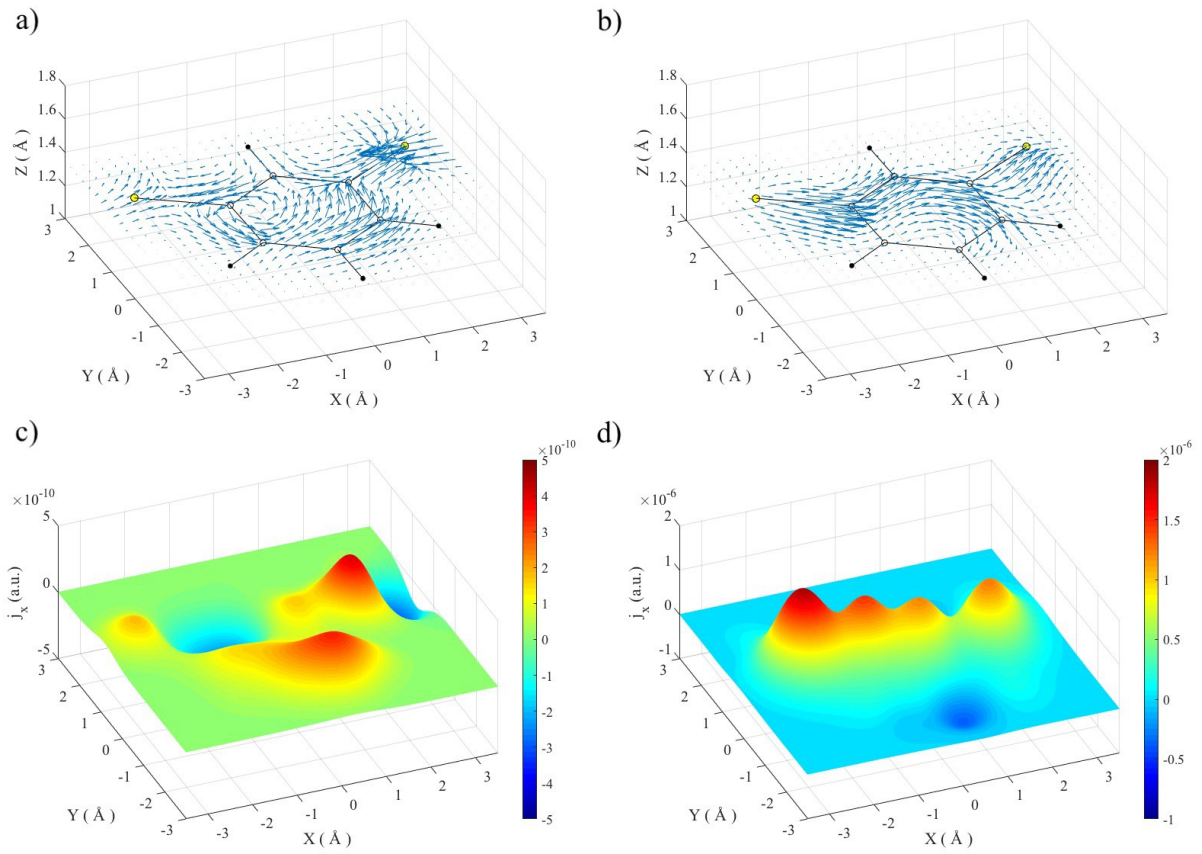

FIG. 5. Inelastic local transport in meta-benzenedithiol (MBDT) molecular junction at $z = 1.32$ Å above molecular plane. Shown are local current vector fields at (a) $V_{sd} = 0.5$ eV and (b) $V_{sd} = 3$ eV (molecular structure is added as a guide to the eye); and maps of flux along the junction (j_x) vs. position in xy plane - (c) and (d) panels, respectively.

significant - see Fig. 3 below) integrated flux through left side of the slab differs from that through right slab side. The difference is due to electronic density production in the slab (compare thick dashed and thin solid lines in the inset). In addition to this physical picture, as discussed above, there is technical issue related to incompleteness of the basis (compare dashed and dotted lines in Fig. 2).

Figure 3 presents local transport characteristics of para-benzenedithiol (PBDT) molecular junction sketched in Fig. 1. A slice of the local current vector field at 1.5 Å above molecular plane is shown in panel (a). One sees that while mostly flux follows the bond structure, non-negligible contribution comes also from wide distribution around bonds and flow through center of the molecular ring. This is particularly clear from the j_x (projection along the

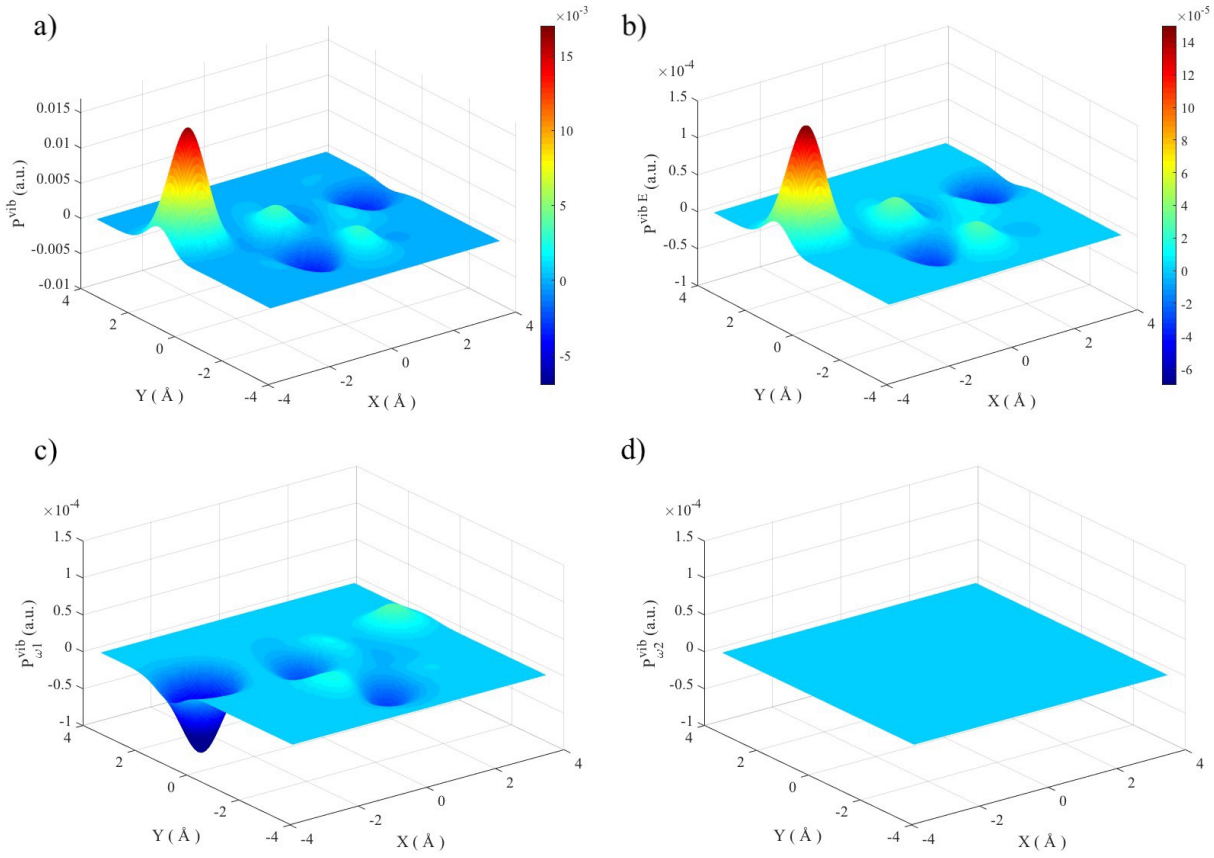

FIG. 6. Map of source term due to electron-vibration interaction in meta-benzenedithiol (MBDT) molecular junction at $z = 1.5$ Å above molecular plane. Shown are (a) electron population redistribution, Eq. (C1); (b) heating/cooling map, Eq. (C8); and electron population redistribution due to interaction with vibrational modes (c) $\omega_1 = 893$ cm^{-1} and (d) $\omega_2 = 1091$ cm^{-1}.

tunneling direction) distribution map in panel (b). Maps of contributions to source term (13) from electron-electron interactions (calculation is preformed at the Hartree-Fock level of theory) and contacts are presented in panels (c) and (d), respectively. Confinement of electron-electron interaction to sulphur atoms can be explained as consequence of relatively weak sulphur-carbon bond, so that injection (elimination) of electrons on the left (right) leads to high localized concentration of electrons (holes), which in turn results in stronger local interactions. Note depletion (accumulation) of electronic density on left (right) carbon atom adjacent to corresponding sulphur (see panel (c) of the figure). It is also quite natural that source term due to contacts is localized in the area of molecule-contacts coupling (see panel d).

Formation of circular currents in meta configuration of benzenedithiol junction was discussed in the literature [29] employing analysis of bond currents in the molecule. We illustrate curl (vortex) formation in local current vector field of meta-benzenedithiol (MBDT) junction in Fig. 4. Here current density yields clear intuitive picture of circular current formation. Due to proximity of contacts source term due to interactions has more complicated structure than in PBDT case (see Fig. 4c). Note that detailed discussion of vortex formation for elastic transport in non-interacting junctions treated within Landauer scattering approach was presented in Refs. [21, 25, 30, 31]. Note also that attempt to utilize source term in calculation of electrostatic field and (proportional to it) current [26, 27] would miss vortex structure.

We now turn to discuss role of molecular vibrations in local current formation. To do this we simulate normal modes of the MBDT junction (after geometry relaxation sulfur atoms are fixed) and evaluate electron-vibration coupling $M^{\alpha}_{m_1m_2}$ for each normal mode α following Ref. [33]. We then employ self-consistent Born approximation [34]

$$\begin{aligned}\Sigma^{int\,vib}_{m_1m_2}(\tau_1,\tau_2) = i\sum_{\alpha}\sum_{m_3,m_4} D_{\alpha}(\tau_1,\tau_2) \\ \times M^{\alpha}_{m_1m_3}\, G_{m_3m_4}(\tau_1,\tau_2)\, M^{\alpha}_{m_4m_2} \\ + i\,\delta(\tau_1,\tau_2)\sum_{\alpha}\sum_{n_1,n_2} M^{\alpha}_{m_1m_2}\, M^{\alpha}_{n_2n_1} \\ \times \int_c d\tau_3\, D^{\alpha}(\tau_1,\tau_3)\, G_{n_1n_2}(\tau_3,\tau_3+)\end{aligned} \tag{17}$$

to account for the interaction. Here $D_{\alpha}(\tau_1,\tau_2)$ is free phonon Green function [35], and deriving (17) we neglected vibrational modes coupling via electronic subsystem of the molecule (see Appendix A for details). The simulation starts by constructing Green function from Gaussian output disregarding electron-vibration interaction. For simplicity we work in molecular orbitals basis. The non-interacting Green function together with phonon propagator, Eqs. (A8) and (A9), is used in Eq. (17) to account for contribution of molecular vibrations. Employing vibrational contribution to total self-energy in the Dyson equation, Eq.(6), updates Green function. The latter is used to update the vibrational self-energy, and the procedure continues in a self-consistent manner. Convergence is assumed when change in population of molecular orbitals in consecutive steps is less than 10^{-6}.

Figure 5 shows effect of decoherence caused by inelastic processes on local current formation in MBDT junction model. While at relatively low bias, $V_{sd} = 0.5$ V, inelastic processes

lead to only slight modifications of the local current flow (compare Figs. 4a and 5a), higher bias, $V_{sd} = 3$ V, effectively destroys vortex structure in the junction (see Figs. 5b and 5d). Note that vortex formation was explained as result of 'topological defects' (lines on which electron wave function is zero and its phase is not defined) in Ref. [28]. We see that vortices disappear when electron coupling to molecular vibrations is taken into account. Note also that analysis of inelastic circular flux using bond currents [16] should be done with caution: while separation of total bond flux into directed and circular components is not unique (additional constraints should be imposed to make the separation unique [29]), similar consideration in the presence of interactions (e.g., electron-vibration coupling) is questionable. Indeed, it is not obvious that dissipation due to interactions remains the same before and after such separation. Thus, in presence of inelastic effects simulating local fluxes is preferable way to study circular currents in junctions.

Finally, we discuss what information one can get from studying source terms. Similar to distinguishing different contributions to the total self-energy, Eq. (7), one can identify separate contributions to the source term (13). Each contribution characterizes electron population exchange with a bath (contact) and/or redistribution in energy due to corresponding interaction. For example, source term due to electron-vibration interaction, P^{vib}, is obtained by substituting self-energy (17) in place of the total self-energy in (13) (see Eq. (C1) in Appendix C). This term yields information on electronic population redistribution on the molecule due to inelastic processes. Figure 6a shows such map for the MBDT junction. We see that for $z = 1.5$ Å population accumulates near source and that majority of inelastic processes happen at the left side of the junction. The latter is in agreement with position of maximum of local electron flux (see Fig. 5d). We note in passing that Integral of $P^{vib}(\vec{r})$ over all the space is zero, because inelastic processes conserve total charge on the molecule.

Another piece of information can be obtained from a modified source term characterizing energy (rather than particle) exchange. Again, taking electron-vibration interaction as an example, one can show that multiplying terms under integral in (A6)-(A7) by frequency ω leads to the modified version of the term, $P^{vib\,E}(\vec{r}, t)$, which characterizes energy exchange between electronic and vibrational subsystems (see Eq. (C8) and corresponding discussion in Appendix C). Figure 6b shows spatial map of the term. This map characterizes local heating/cooling of the molecule due to inelastic effects. We see that in agreement with

population accumulation heating takes place also mostly near source.

One can also explore mode resolved maps; they are obtained by choosing particular α in (A6)-(A7) for particle redistribution (or (C6)-(C7) for heating/cooling). Figures 6c and 6d show two examples for population redistribution due to interaction with vibrational modes $\omega_1 = 893$ cm^{-1} and $\omega_2 = 1091$ cm^{-1}. One sees that while mode ω_1 has significant influence on electron transport, mode ω_2 practically does not contribute. The reason is longitudinal motion (motion along direction of current) caused by mode ω_1 and mostly perpendicular atomic displacements caused by mode ω_2. Thus the former couples strongly to tunneling electron, while the latter is almost decoupled. The effect is due to the former mode causing longitudinal motion . It is interesting to note, that contrary to the total population redistribution, mode ω_1 leads to depletion of population near source.

Similarly, expressions for source term due to coupling to contacts would describe particle and/or energy flux between electronic baths and molecule. In an extended model, this may be used to describe molecular interactions with plasmonic and/or electron-hole excitations in the contacts. We postpone these studies for future research.

IV. CONCLUSION

We present pedagogical review of current density (local current) simulation in molecular junctions. Local transport characteristics in junctions are most often studied with bond currents. Contrary to the latter, local currents are capable to provide much richer local transport information. At the same time, simulation of local currents should be done and analyzed with care: such simulations are sensitive to choice of the basis and electronic structure method. In particular, density functional theory is not always applicable in local current simulations because DFT does not provide energy resolution fro self-energy due to interactions, which may lead to qualitative failures even in prediction of total fluxes (quantities much less sensitive to details of simulation than current density). Incompleteness of basis in quantum chemistry calculations is another complication to be taken into account. We note that conservation of local current within the molecule should account for source terms due to open character of the junction and due to intra-molecular interactions. We illustrate our discussions by simulating elastic and inelastic local currents in benzenedithiol junction. We show that local flux does not necessarily follow molecular bonds with significant part of

the flux going 'through space'. In meta-connected benzenedithiol we illustrate formation of vortex structure (circular local current). We also show how molecular vibrations introducing decoherence effectively eliminate vortex formation in the local current map. Finally, we discuss information one can get from studying source terms. We defer further investigation of inelastic effects on local junction properties (inelastic current and local heating, polaron formation and charge localization, current induced chemistry) in realistic systems to future research.

ACKNOWLEDGMENTS

MG research is supported by the National Science Foundation (CHE-1565939) and the US Department of Energy (DE-SC0018201). AJ thanks Gemma Solomon for financial support during his visit to UC San Diego.

Appendix A: Electron self-energies

Here we give explicit expressions for self-energies utilized in the simulations. The contribution to total self-energy (7) due to coupling to contacts ($K = L, R$) can be evaluated exactly

$$\Sigma^K_{m_1 m_2}(\tau_1, \tau_2) = \sum_{k \in K} V_{m_1 k}\, g_k(\tau_1, \tau_2)\, V_{k m_2} \tag{A1}$$

Here $g_k(\tau_1, \tau_2) = -i\langle T_c\, \hat{c}_k(\tau_1)\, \hat{c}^\dagger_k(\tau_2)\rangle$ is free electron Green function in state k of contact K. At steady-state, Fourier transforms of its lesser and retarded projections are

$$\Sigma^{K\,<}_{m_1 m_2}(E) = i\,\Gamma^K_{m_1 m_2}\, f_K(E) \tag{A2}$$

$$\Sigma^{K\,r}_{m_1 m_2}(E) = \Lambda^K_{m_1 m_2}(E) - \frac{i}{2}\Gamma^K_{m_1 m_2}(E) \tag{A3}$$

Here $f_K(E) = [exp(\frac{E-\mu_K}{k_B T}) + 1]^{-1}$ is the Fermi-Dirac thermal distribution, and

$$\Lambda^K_{m_1 m_2}(E) = \mathrm{PP} \int \frac{dE'}{2\pi}\, \frac{\Gamma^K_{m_1 m_2}(E')}{E - E'} \tag{A4}$$

$$\Gamma^K_{m_1 m_2}(E) = 2\pi \sum_{k \in K} V_{m_1 k}\, V_{k m_2}\, \delta(E - \varepsilon_k) \tag{A5}$$

are the Lamb shift and dissipation of molecular electronic states due to coupling to contact K. In our calculations we employ the wide band approximation [35] for which $\Lambda^K = 0$ and Γ^K does not depend on energy.

At steady state, retarded and lesser projections of electronic self-energy due to coupling to molecular vibrations $\{\alpha\}$, Eq. (17), are [36, 37]

$$\Sigma^{int\,vib\,<}_{m_1m_2}(E) = i\sum_{\alpha}\sum_{n_1,n_2}\int\frac{d\omega}{2\pi}D^{<}_{\alpha}(\omega) \tag{A6}$$

$$\times\, M^{\alpha}_{m_1n_1}\, G^{<}_{n_1n_2}(E-\omega)\, M^{\alpha}_{n_2m_2}$$

$$\Sigma^{int\,vib\,r}_{m_1m_2}(E) = i\sum_{\alpha}\sum_{n_1,n_2}\int\frac{d\omega}{2\pi}M^{\alpha}_{m_1n_1}M^{\alpha}_{n_2m_2} \tag{A7}$$

$$\times\Big(D^{<}_{\alpha}(\omega)\,G^{r}_{n_1n_2}(E-\omega) + D^{r}_{\alpha}(\omega)\,G^{<}_{n_1n_2}(E-\omega)$$

$$+\, D^{r}_{\alpha}(\omega)\,G^{r}_{n_1n_2}(E-\omega)\Big)$$

$$-\,i\sum_{\alpha}M^{\alpha}_{m_1m_2}D^{r}_{\alpha}(\omega=0)\sum_{n_1,n_2}M^{\alpha}_{n_2n_1}\int\frac{dE'}{2\pi}\,G^{<}_{n_1n_2}(E')$$

In the simulations we disregarded reorganization of molecular levels due to electron-vibration interaction. Note, it can be easily included, but for relatively weak coupling does not play an important role. Vibrational modes where assumed to be free harmonic oscillators in equilibrium

$$D^{<}_{\alpha}(\omega) = -2\pi i\Big(N(\omega)\delta(\omega-\omega_\alpha) + [1+N(\omega)]\delta(\omega+\omega_\alpha)\Big) \tag{A8}$$

$$D^{r}_{\alpha}(\omega) = \frac{1}{\omega-\omega_\alpha+i\delta} - \frac{1}{\omega+\omega_\alpha+i\delta} \tag{A9}$$

Here $N(\omega) = [\exp\frac{\hbar\omega}{k_BT}-1]^{-1}$ is the Bose-Einstein thermal distribution and $\delta\to 0+$.

Finally, as discussed in the text, self-energy due to electron-electron interactions, $\Sigma^{int\,HF}$, was obtained numerically from the Gaussian [32] output.

Appendix B: Derivation of Eq. (10)

Here we derive continuity equation (10) starting from the left-side Dyson equation (6) and its right-side analog

$$\mathbf{G}(\tau_1,\tau_2)\Big(-i\overleftarrow{\partial}_{\tau_2}\mathbf{I} - \mathbf{H}^{(0)}_{M}\Big) = \tag{B1}$$

$$\delta(\tau_1,\tau_2)\,\mathbf{I} + \int_c d\tau_3\,\mathbf{G}(\tau_1,\tau_3)\,\Sigma(\tau_3,\tau_2)$$

Their lesser projections are [36]

$$\Big(i\,\partial_{t_1}\,\mathbf{I}-\mathbf{H}_M^{(0)}\Big)\mathbf{G}^<(t_1,t_2)= \tag{B2}$$
$$\int_{-\infty}^{+\infty}dt_3\Big(\Sigma^<(t_1,t_3)\,\mathbf{G}^a(t_3,t_2)+\Sigma^r(t_1,t_3)\,\mathbf{G}^<(t_3,t_2)\Big)$$
$$\mathbf{G}^<(t_1,t_2)\Big(-i\overleftarrow{\partial}_{t_2}\mathbf{I}-\mathbf{H}_M^{(0)}\Big)= \tag{B3}$$
$$\int_{-\infty}^{+\infty}dt_3\Big(\mathbf{G}^<(t_1,t_3)\,\Sigma^a(t_3,t_2)+\mathbf{G}^r(t_1,t_3)\,\Sigma^<(t_3,t_2)\Big)$$

Subtracting (B2) from (B3) and taking $t_1=t_2\equiv t$ leads to

$$-i\,d_t\,\mathbf{G}^<(t,t)+\Big[\mathbf{H}_M^{(0)};\mathbf{G}^<(t,t)\Big]= \tag{B4}$$
$$2\,\mathrm{Re}\int_{-\infty}^{+\infty}dt_3\Big(\mathbf{G}^<(t,t_3)\,\Sigma^a(t_3,t)+\mathbf{G}^r(t,t_3)\,\Sigma^<(t_3,t)\Big)$$

Assuming real space basis in (B4), utilizing

$$H_M^{(0)}(\vec{r}_1,\vec{r}_2)=\delta(\vec{r}_1-\vec{r}_2)\Big(-\frac{1}{2}\Delta_{r_1}+V(\vec{r}_1)\Big), \tag{B5}$$

and taking $\vec{r}_1=\vec{r}_2\equiv\vec{r}$ leads to (10).

Appendix C: Local heating and cooling

Here we discuss connection of the electron-vibration source term

$$P^{vib}(\vec{r},t)=2\,\mathrm{Re}\int d\vec{r}_1\int dt_1 \tag{C1}$$
$$\Big(G^<(\vec{r},t;\vec{r}_1,t_1)\,\Sigma^{int\,vib\,a}(\vec{r}_1,t_1;\vec{r},t)$$
$$+\,G^r(\vec{r},t;\vec{r}_1,t_1)\,\Sigma^{int\,vib\,<}(\vec{r}_1,t_1;\vec{r},t)\Big)$$

to particle flux and local heating/cooling in the molecule. Utilizing relations between Green function projections (similar relations hold for self-energy projections)

$$G^r(\vec{r}_1,t_1;\vec{r}_2,t_2)= \tag{C2}$$
$$\theta(t_1-t_2)\Big(G^>(\vec{r}_1,t_1;\vec{r}_2,t_2)-G^<(\vec{r}_1,t_1;\vec{r}_2,t_2)\Big)$$
$$G^a(\vec{r}_1,t_1;\vec{r}_2,t_2)= \tag{C3}$$
$$\theta(t_2-t_1)\Big(G^<(\vec{r}_1,t_1;\vec{r}_2,t_2)-G^>(\vec{r}_1,t_1;\vec{r}_2,t_2)\Big)$$

one identifies (C1) as space-resolved contribution to vertical flux [38]

$$I^{vib}(t) = \int d\vec{r}\, I^{vib}(\vec{r},t) \tag{C4}$$

$$I^{vib}(\vec{r},t) = 2\,\mathrm{Re}\int d\vec{r}_1 \int_{-\infty}^{t} dt_1 \tag{C5}$$
$$\Big(\Sigma^{int\,vib<}(\vec{r},t;\vec{r}_1,t_1)\, G^{>}(\vec{r}_1,t_1;\vec{r},t)$$
$$- \Sigma^{int\,vib>}(\vec{r},t;\vec{r}_1,t_1)\, G^{<}(\vec{r}_1,t_1;\vec{r},t) \Big)$$

Total vertical flux $I^{vib}(t)$ is zero because interaction with vibrations conserves charge of the molecule. At the same time, its spatial distribution $P^{vib}(\vec{r},t) \equiv I^{vib}(\vec{r},t)$ yields information on electron population reshuffling on the molecule due to inelastic effects.

It is clear, that electronic population redistribution is accompanied by creation/destruction of vibrational quanta. Note in passing that for total flux one can formally show equivalence of vertical flux into electronic subsystem and phonon flux out of molecular vibrations; this is direct consequence of common source (the Luttinger-Ward functional [39, 40]) for electron self-energy due to coupling to vibrations and vibrational self-energy due to coupling to electrons. Creation (destruction) of vibrational quanta results also in energy exchange between electron and vibrational degrees of freedom. To account for energy exchange one has to modify self-energy eexpressions (A6)-(A7) to account for energy (rather than particle) exchange. This is done including ω under integral over frequency

$$\Sigma^{vib\,E<}_{m_1m_2}(E) = i\sum_{\alpha}\sum_{n_1,n_2}\int \frac{d\omega}{2\pi}\,\omega\, D^{<}_{\alpha}(\omega) \tag{C6}$$
$$\times\, M^{\alpha}_{m_1n_1}\, G^{<}_{n_1n_2}(E-\omega)\, M^{\alpha}_{n_2m_2}$$

$$\Sigma^{vib\,E\,r}_{m_1m_2}(E) = i\sum_{\alpha}\sum_{n_1,n_2}\int \frac{d\omega}{2\pi}\,\omega\, M^{\alpha}_{m_1n_1} M^{\alpha}_{n_2m_2} \tag{C7}$$
$$\times \Big(D^{<}_{\alpha}(\omega)\, G^{r}_{n_1n_2}(E-\omega) + D^{r}_{\alpha}(\omega)\, G^{<}_{n_1n_2}(E-\omega)$$
$$+ D^{r}_{\alpha}(\omega)\, G^{r}_{n_1n_2}(E-\omega) \Big)$$

Using these expressions in (C1) yields modified version of the source term

$$P^{vib\,E}(\vec{r},t) = 2\,\mathrm{Re}\int d\vec{r}_1 \int dt_1 \left(G^{<}(\vec{r},t;\vec{r}_1,t_1)\,\Sigma^{vib\,E\,a}(\vec{r}_1,t_1;\vec{r},t) + G^{r}(\vec{r},t;\vec{r}_1,t_1)\,\Sigma^{vib\,E\,<}(\vec{r}_1,t_1;\vec{r},t) \right) \tag{C8}$$

which characterizes spatially resolved heating/cooling of the molecule due to inelastic processes.

---

[1] A. Aviram and M. A. Ratner, Chem. Phys. Lett. **29**, 277 (1974).

[2] N. J. Tao, Nature Nanotech. **1**, 173 (2006).

[3] Z. Huang, B. Xu, Y. Chen, M. Di Ventra, and N. Tao, Nano Lett. **6**, 1240 (2006).

[4] Z. Huang, F. Chen, R. D'agosta, P. A. Bennett, M. Di Ventra, and N. Tao, Nature Nanotech. **2**, 698 (2007).

[5] M. Tsutsui, M. Taniguchi, and T. Kawai, Nano Lett. **8**, 3293 (2008), pMID: 18729417.

[6] Y. Dubi and M. Di Ventra, Nano Lett. **9**, 97 (2009).

[7] Y. Dubi and M. Di Ventra, Rev. Mod. Phys. **83**, 131 (2011).

[8] Z. Ioffe, T. Shamai, A. Ophir, G. Noy, I. Yutsis, K. Kfir, O. Cheshnovsky, and Y. Selzer, Nature Nanotech. **3**, 727 (2008).

[9] D. R. Ward, D. A. Corley, J. M. Tour, and D. Natelson, Nature Nanotech. **6**, 33 (2011).

[10] J. Zhang, P. Chen, B. Yuan, W. Ji, Z. Cheng, and X. Qiu, Science **342**, 611 (2013).

[11] C.-l. Chiang, C. Xu, Z. Han, and W. Ho, Science **344**, 885 (2014).

[12] Y. Zhang, Y. Luo, Y. Zhang, Y.-J. Yu, Y.-M. Kuang, L. Zhang, Q.-S. Meng, Y. Luo, J.-L. Yang, Z.-C. Dong, and J. G. Hou, Nature **531**, 623 (2016).

[13] A. A. Stuchebrukhov, J. Chem. Phys. **104**, 8424 (1996).

[14] T. N. Todorov, Journal of Physics: Condensed Matter **14**, 3049 (2002).

[15] G. C. Solomon, C. Herrmann, T. Hansen, V. Mujica, and M. A. Ratner, Nature Chem. **2**, 223 (2010).

[16] D. Rai and M. Galperin, Phys. Rev. B **86**, 045420 (2012).

[17] H. K. Yadalam and U. Harbola, Phys. Rev. B **94**, 115424 (2016).

[18] T. Hansen, G. C. Solomon, and T. Hansen, J. Chem. Phys. **146**, 092322 (2017).

[19] S.-M. Jhan and B.-Y. Jin, J. Chem. Phys. **147**, 194106 (2017).

[20] Y. Xue and M. A. Ratner, Phys. Rev. B **70**, 081404 (2004).

[21] D. Nozaki and W. G. Schmidt, J. Comp. Chem. **38**, 1685 (2017).

[22] A. Baratz, M. Galperin, and R. Baer, J. Phys. Chem. C **117**, 10257 (2013).

[23] A. Baratz, M. Galperin, and R. Baer, J. Phys. Chem. C **117**, 18279 (2013).

[24] P. Holland, Annalen der Physik **12**, 446 (2003).

[25] M. Walz, A. Bagrets, and F. Evers, J. Chem. Theory Comput. **11**, 5161 (2015), pMID: 26574313, https://doi.org/10.1021/acs.jctc.5b00471.

[26] C. Li, L. Wan, Y. Wei, and J. Wang, Nanotechnology **19**, 155401 (2008).

[27] L. Zhang, B. Wang, and J. Wang, Phys. Rev. B **84**, 115412 (2011).

[28] I. Daizadeh, J. xin Guo, and A. Stuchebrukhov, J. Chem. Phys. **110**, 8865 (1999).

[29] D. Rai, O. Hod, and A. Nitzan, J. Phys. Chem. C **114**, 20583 (2010).

[30] M. Walz, J. Wilhelm, and F. Evers, Phys. Rev. Lett. **113**, 136602 (2014).

[31] J. Wilhelm, M. Walz, and F. Evers, Phys. Rev. B **92**, 014405 (2015).

[32] M. J. Frisch, G. W. Trucks, H. B. Schlegel, G. E. Scuseria, M. A. Robb, J. R. Cheeseman, G. Scalmani, V. Barone, G. A. Petersson, H. Nakatsuji, X. Li, M. Caricato, A. V. Marenich, J. Bloino, B. G. Janesko, R. Gomperts, B. Mennucci, H. P. Hratchian, J. V. Ortiz, A. F. Izmaylov, J. L. Sonnenberg, D. Williams-Young, F. Ding, F. Lipparini, F. Egidi, J. Goings, B. Peng, A. Petrone, T. Henderson, D. Ranasinghe, V. G. Zakrzewski, J. Gao, N. Rega, G. Zheng, W. Liang, M. Hada, M. Ehara, K. Toyota, R. Fukuda, J. Hasegawa, M. Ishida, T. Nakajima, Y. Honda, O. Kitao, H. Nakai, T. Vreven, K. Throssell, J. A. Montgomery, Jr., J. E. Peralta, F. Ogliaro, M. J. Bearpark, J. J. Heyd, E. N. Brothers, K. N. Kudin, V. N. Staroverov, T. A. Keith, R. Kobayashi, J. Normand, K. Raghavachari, A. P. Rendell, J. C. Burant, S. S. Iyengar, J. Tomasi, M. Cossi, J. M. Millam, M. Klene, C. Adamo, R. Cammi, J. W. Ochterski, R. L. Martin, K. Morokuma, O. Farkas, J. B. Foresman, and D. J. Fox, "Gaussian09, Revision C.01," (2016), gaussian Inc. Wallingford CT.

[33] N. Sergueev, D. Roubtsov, and H. Guo, Phys. Rev. Lett. **95**, 146803 (2005).

[34] T.-H. Park and M. Galperin, Phys. Rev. B **84**, 205450 (2011).

[35] G. D. Mahan, *Many-Particle Physics* (Plenum Press, 1990).

[36] H. Haug and A.-P. Jauho, *Quantum Kinetics in Transport and Optics of Semiconductors*,

second, substantially revised edition ed. (Springer, Berlin Heidelberg, 2008).

[37] M. Galperin, M. A. Ratner, and A. Nitzan, J. Chem. Phys. **121**, 11965 (2004).

[38] S. Datta, *Electronic Transport in Mescoscopic Systems* (Cambridge University Press, 1995).

[39] J. M. Luttinger and J. C. Ward, Phys. Rev. **118**, 1417 (1960).

[40] Y. Gao and M. Galperin, J. Chem. Phys. **144**, 174113 (2016).